MULTIPLE CRACK DAMAGE DETECTION OF STRUCTURES USING SIMPLIFIED PZT MODEL

Narayanan Jinesh and Krishnapillai Shankar

msp

MULTIPLE CRACK DAMAGE DETECTION OF STRUCTURES USING SIMPLIFIED PZT MODEL

NARAYANAN JINESH AND KRISHNAPILLAI SHANKAR

A novel damage identification scheme for multiple cracks in beams is presented based on the one-dimensional (1-D) piezoelectric patch with beam model. A hybrid element constituted of a 1-D beam element and a PZT sensor is used with reduced material properties. This model is more convenient and simpler for crack identification of beams than using a complex 3-D patch model. The hybrid beam element and the multiple crack identification procedure is verified experimentally. The crack identification is carried out as an inverse problem whereby location and depth parameters are identified by minimizing the deviation between the predicted and measured voltage responses of the patch when subjected to excitations. In the proposed method, a patch is attached to either end of the fixed beam. The numerical and experimental results show that there is significant improvement in identification accuracy compared to other methods.

1. Introduction

Structural health monitoring (SHM) is the process in which the state of structural health is directly assessed using a nondestructive approach. Damage occurs during service because of the operational cyclic loading, aging, mechanical vibration, changing ambient conditions, shocks, and chemical attack. Hence, the early detection of damage, location, and its severity is very important in the current scenario. Generally, damage identification methods such as acoustic, radiography, magnetic field, and thermal field methods are used for damage detection. All of these techniques are expensive and require that the zone of the damage is known a priori and the structural element being inspected is readily accessible. As an alternative, vibration-based damage detection methods using the inverse concept deserve further investigation.

A crack in a structural element increases the local flexibility, which is a function of crack depth and location. Lee and Shin [2002] identified the location and magnitude of local damage of a beam structure from the dynamic stiffness equation of the beam structure. In that paper, experimentally measured frequency response function data from the damage structure were required as the input data and applicability was limited to cases for which exact dynamic stiffness matrices are obtainable. Yang and Wang [2010] introduced a new damage detection method based on the concept of a natural frequency vector (NFV) and the natural frequency vector assurance criterion (NFVAC), which was verified by both simulative and experimental examples. Wang et al. [2001] suggested a two-stage identification algorithm utilizing changes in natural frequencies and static displacements for identifying structural damage. Liu et al. [2011] identified the presence of structural damage using multiobjective optimization, keeping variations in natural frequency and mode shapes as individual objective functions. Viola et al. [2001] formulated shape functions of a cracked Timoshenko beam element based on the Hamilton principle,

with crack sections represented as elastic hinges. A nondestructive evaluation procedure for identifying the magnitude and location of the structure based on experimentally measured frequency and mode shape was developed. Viola et al. [2002] investigated the effect of cracks in the stiffness matrix which neglect the crack closure effect by assuming an open crack.

Patil and Maiti [2005] predicted the location and size of multiple cracks on a slender beam based on experimentally measured frequencies. A strategy to overcome failure in the prediction for cases where one of the cracks is located near an antinode was presented. Douka et al. [2004] investigated the effect of two transverse cracks on the mechanical impedance of a double-cracked cantilever beam both analytically and experimentally. They found significant change of antiresonance frequency due to the presence of cracks, and this additional information was used along with natural frequency changes to identify cracks. Ding et al. [2017] identified multiple cracks using the improved artificial bee colony algorithm (I-ABC) based on an objective function which consists of a limited number of measured natural frequencies. Sekhar [2008] reviewed multiple crack identification in beam, rotor, and pipe structures. The aforementioned study summarized the effects, modeling of cracks, and various vibration identification methods for multiple cracks. Sinha et al. [2002] developed a multicrack model in an Euler–Bernoulli beam based on a small modification of the local flexibility in the vicinity of the crack. In that paper, crack models were incorporated into the finite element model of the structure, and crack location and size were estimated using the model updating from the experimentally measured modal data.

Philips Adewuyi et al. [2009] identified single/multiple damage in beam using the combined measurement of displacement modes from an accelerometer and distributed strain modes with fiber Bragg grating (FBG) sensors. Nandakumar and Shankar [2014] identified multiple crack parameters in the beam using the concept of double-crack transfer matrices with the combined measurements of an accelerometer and a strain gauge. Verhese and Shankar [2014] applied the combined instantaneous power flow balance and conventional acceleration matching concept for the substructural identification of multiple crack parameters of the beam. In the above described method, accelerometers were used as sensors for structural parameter identification.

The high reliability, sensitivity, and electromechanical coupling property of PZT has gained significant attention for potential application as sensors for structural health monitoring. Bendary et al. [2010] formulated a one-dimensional integrated beam element using Hermite cubic and Lagrangian interpolation functions which are carried out for static and dynamic analysis. Zemčík and Sadílek [2007] developed the one-dimensional hybrid PZT element based on the Euler–Bernoulli beam using the bilinear Lagrangian interpolation polynomial for electric potential which is carried out for modal analysis. Later, the same element was used for frequency response analysis and the results were experimentally verified in [Sadílek and Zemčík 2010]. Sulbhewar and Raveendranath [2015] formulated the one-dimensional Euler–Bernoulli beam with PZT structure using a coupled field polynomial that is independent of the material configuration of the piezoelectric beam cross section. A two-stage identification strategy was proposed by Fukunaga et al. [2002] using a limited number of PZT sensors in the time and frequency domain. It identified crack depth up to 10% depth, but it strongly depends on reliable modal data of undamaged structure.

In most of the literature available, accelerometer signals are used for structural identification. However, compared to accelerometers, PZT patches have the advantages of low cost with negligible weight and wide dynamic range. The most notable feature of PZT patches is their miniaturized appearance and ability

to be implanted in civil structures for in situ health monitoring of the structure. Moreover, because of their light weight, PZT patches are not likely to alter the dynamic properties, and their output voltage is less likely to be contaminated with signal noise. In the present proposed method, an integrated beam structure with a PZT sensor is incorporated into the finite element model of the structure and is used for the direct identification of damage at various locations in structure. Damage identification using a one-dimensional piezobeam hybrid model is not reported in the literature. Hence, it is a novel contribution. The objective function consists of the mean square of the deviation between measured and estimated voltage from the PZT patches. Multiple crack identification using the one-dimensional PZT patch model and the effect of patch length are not reported in the literature. The one-dimensional hybrid element is especially convenient and simple for modeling beam-type structures as compared to more complex 3-D PZT patch models. The computational complexity is significantly reduced using a one-dimensional element. The theory is validated with numerical and experimental examples in the sections below.

2. Constitutive equations of PZT

Piezoelectric materials transform mechanical displacement into an electrical field (voltage potential), in which case the piezoelectric material acts as a sensor (direct effect), and its converse effect acts as an actuator. The constitutive equations for the transversely isotropic piezoelectric medium which define the interaction between the stress (σ), strain (ε), electric displacement (D), and electric field (E) are of the form [Benjeddou 2000]

$$\sigma_j = C_{jk}\varepsilon_k - e_{jm}E_m, \tag{1}$$

$$D_l = e_{lj}\varepsilon_k + \epsilon_{lm}E_m, \tag{2}$$

where C_{jk}, ϵ_{lm}, and e_{lj} ($j, k = 1, \ldots, 6$ and $l, m = 1, \ldots, 3$) are the elastic, dielectric, and piezoelectric coupling coefficients, respectively. The transversely poled piezoelectric material is bonded/embedded in the host structure. The complete coupled three dimensional constitutive equation of a piezoelectric material with principal material axes (x, y and z) can be written as [Sulbhewar and Raveendranath 2015]

$$
\begin{bmatrix}
\sigma_x \\
\sigma_y \\
\sigma_z \\
\tau_{yz} \\
\tau_{xz} \\
\tau_{xy} \\
D_x \\
D_y \\
D_z
\end{bmatrix}
=
\begin{bmatrix}
C_{11} & C_{12} & C_{13} & 0 & 0 & 0 & 0 & 0 & -e_{31} \\
C_{12} & C_{22} & C_{23} & 0 & 0 & 0 & 0 & 0 & -e_{32} \\
C_{13} & C_{23} & C_{33} & 0 & 0 & 0 & 0 & 0 & -e_{33} \\
0 & 0 & 0 & C_{44} & 0 & 0 & 0 & -e_{24} & 0 \\
0 & 0 & 0 & 0 & C_{55} & 0 & -e_{15} & 0 & 0 \\
0 & 0 & 0 & 0 & 0 & C_{66} & 0 & 0 & 0 \\
0 & 0 & 0 & 0 & e_{15} & 0 & \epsilon_{11} & 0 & e_{32} \\
0 & 0 & 0 & e_{24} & 0 & 0 & 0 & \epsilon_{22} & 0 \\
e_{31} & e_{32} & e_{33} & 0 & 0 & 0 & 0 & 0 & \epsilon_{33}
\end{bmatrix}
\begin{bmatrix}
\varepsilon_x \\
\varepsilon_y \\
\varepsilon_z \\
\gamma_{yz} \\
\gamma_{xz} \\
\gamma_{xy} \\
E_x \\
E_y \\
E_z
\end{bmatrix},
\tag{3}
$$

where τ and γ are shear stress and shear strain, respectively.

3. One-dimensional beam geometry

The three-dimensional beam with axes is shown in Figure 1. The Euler–Bernoulli beam theory is applied for a one-dimensional beam with a piezoelectric patch, which neglects the shear effect. The model is

assumed to be plane stress and width in the y-direction is stress free. Therefore, it is possible to set $\sigma_y = \sigma_z = \tau_{xy} = \tau_{xz} = \tau_{yz} = \gamma_{xy} = \gamma_{xz} = \gamma_{yz} = 0$ while $\varepsilon_y \neq 0$, $\varepsilon_z \neq 0$ [Sulbhewar and Raveendranath 2015]. The polarization axis z is aligned with the thickness direction of the beam, thus only D_z is taken and for electric field $E_x = E_y = 0$. Applying these conditions, (3) is reduced to the form

$$\begin{bmatrix} \sigma_x \\ D_z \end{bmatrix} = \begin{bmatrix} \hat{C} & -\hat{e} \\ \hat{e} & \hat{\epsilon} \end{bmatrix} \begin{bmatrix} \varepsilon_x \\ E_z \end{bmatrix}, \tag{4}$$

where $\hat{C} = Q_{11} - Q_{12}^2/Q_{22}$ and $Q_{ij} = C_{ij} - C_{i3}C_{j3}/C_{33}$ $(i, j = 1, 2)$; $\hat{e} = \bar{e}_{31} - \bar{e}_{32}(Q_{12}/Q_{22})$ and $\bar{e}_{3i} = e_{3i} - e_{33}(C_{13}/C_{33})$ $(i = 1, 2)$; $\hat{\epsilon} = \bar{\epsilon}_{33} + \bar{e}_{32}^2/Q_{22}$ and $\bar{\epsilon}_{33} = \epsilon_{33} + e_{32}^2/C_{33}$ [Kapuria and Hagedorn 2007]. Here, $\hat{C}$, $\hat{\epsilon}$, and $\hat{e}$ are the reduced elastic, dielectric, and piezoelectric coupling coefficients respectively and the calculated values are shown in Table 1. This reduced property is used for further numerical study of the one-dimensional (1-D) beam with a PZT patch in MATLAB.
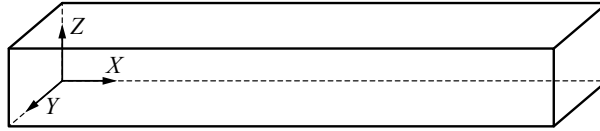

Figure 1. Three-dimensional beam.

material	properties	
aluminum	$E = 71\,\text{GPa}$ $v = 0.3$ $\rho = 2210\,\text{kg} \cdot \text{m}^{-3}$	
PZT 5H	$C_{11} = C_{22} = 126\,\text{GPa}$	$C_{12} = 79.5\,\text{GPa}$
	$C_{13} = C_{23} = 84.1\,\text{GPa}$	$C_{33} = 117\,\text{GPa}$
	$C_{44} = C_{55} = 23\,\text{GPa}$	$C_{66} = 23.25\,\text{GPa}$
	$e_{31} = e_{32} = -6.5\,\text{C} \cdot \text{m}^{-2}$	$e_{33} = 23.3$
	$e_{15} = e_{24} = 17\,\text{C} \cdot \text{m}^{-2}$	$\epsilon_{11} = \epsilon_{22} = 1.503 \times 10^{-8}\,\text{F} \cdot \text{m}^{-1}$
	$\epsilon_{33} = 1.3 \times 10^{-8}\,\text{F} \cdot \text{m}^{-1}$	$\rho = 7500\,\text{kg} \cdot \text{m}^{-3}$
reduced properties	$\hat{C} = 60.013\,\text{GPa}$ $\hat{e} = -16.4921\,\text{C} \cdot \text{m}^{-2}$ $\hat{\epsilon} = 2.5885 \times 10^{-8}\,\text{F} \cdot \text{m}^{-1}$	

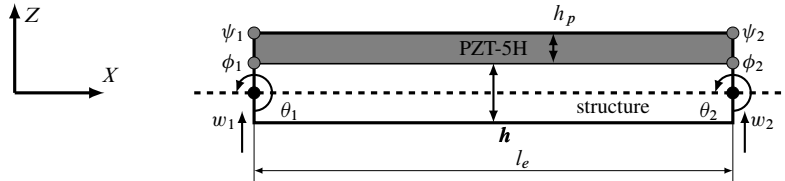**Table 1.** Material properties of the beam.

Figure 2. One-dimensional beam element: PZT and supporting structure sharing common nodes.

4. FEM formulation and elemental matrices

The one-dimensional beam formulation has been presented in [Sadílek and Zemčík 2010; Sulbhewar and Raveendranath 2015], but not used for time domain dynamic response with damping and inverse problems. The finite element formulation of the structure is briefly explained here. The beam element is based on the Euler–Bernoulli theory and the element has two nodes. Two independent polynomials are used for interpolation of mechanical and electrical field variables. First, the Hermite cubic polynomial is used for the interpolation of mechanical quantities of vertical displacement (w) and rotation (θ) as shown in Figure 2. The vertical displacement (w) is approximated across the length as

$$w(x) = a_0 + a_1 x + a_2 x^2 + a_3 x^3 = [N_w]\{w^e\}, \tag{5}$$

where N_w is the shape interpolation function of the structural part and structural nodal degree of freedom per element is arranged as $w^e = [w_1, \theta_1, w_2, \theta_2]^T$. The bending strain is

$$\varepsilon(x, z) = \frac{\partial u}{\partial x} = -z\frac{\partial^2 w}{\partial x^2} = [B_w]\{w^e\}, \tag{6}$$

where $[B_w]$ is the strain-displacement matrix consisting of derivatives of shape functions.

The electric potential is $\phi(x, z)$, considered as a function of the thickness and the length of the beam. Hence, let Langrangian bilinear function be estimated for the interpolation as

$$\phi(x, z) = a_4 + a_5 x + a_6 z + a_7 xz = [\Phi_\phi]\{\phi^e\}. \tag{7}$$

Here, ϕ and ψ are the lower and upper electrical potentials of PZT surface. The electrical nodal degrees of freedom per element can be ordered as $\{\phi^e\} = [\phi_1, \psi_1, \phi_2, \psi_2]^T$. The electric field $E(x, z)$ can be written as

$$E(x, z) = [B_\phi]\{\phi^e\}, \tag{8}$$

where $[B_\phi]$ is the electrical field potential matrix consisting of derivatives of shape functions.

Here, a homogeneous electrical boundary condition is imposed on the bottom surface of PZT patch to eliminate rigid body modes, i.e., the lower surface is grounded with $\phi = 0\,\text{V}$, while the upper surface is left open. The dynamic potential energy density G for the piezoelectric medium can be written as [Xu and ShengPeng 2013]

$$G = \tfrac{1}{2}\varepsilon^T c\varepsilon - \tfrac{1}{2}E^T \epsilon E - \varepsilon^T eE. \tag{9}$$

The elemental matrices are calculated by applying the variational principle to potential, kinetic energy, and external forces (mechanical and electrical loading). This must be satisfied for any arbitrary variation of the displacements and electrical potentials and thus the equations of motion of elemental matrices with damping can be represented as

$$\begin{bmatrix} [M_{ww}^e] & [0] \\ [0] & [0] \end{bmatrix} \begin{Bmatrix} \{\ddot{w}^e\} \\ \{\ddot{\phi}^e\} \end{Bmatrix} + \begin{bmatrix} [C_{ww}^e] & [0] \\ [0] & [0] \end{bmatrix} \begin{Bmatrix} \{\dot{w}^e\} \\ \{\dot{\phi}^e\} \end{Bmatrix} + \begin{bmatrix} [K_{ww}^e] & [K_{w\phi}^e] \\ [K_{w\phi}^e]^T & [K_{\phi\phi}^e] \end{bmatrix} \begin{Bmatrix} \{w^e\} \\ \{\phi^e\} \end{Bmatrix} = \begin{Bmatrix} \{F^e\} \\ \{Q^e\} \end{Bmatrix}. \tag{10}$$

The damping matrix $[C_{ww}^e]$ is defined as a proportional damping, i.e., $[C_{ww}^e] = \alpha[M_{ww}^e] + \beta[K_{ww}^e]$ and α, β are Rayleigh's damping coefficients. Equation (10) is the elemental equilibrium in the discretized form, where $[M_{ww}^e]$ is the mass matrix, and $[K_{ww}^e]$, $[K_{w\phi}^e]$, and $[K_{w\phi}^e]$ are the stiffness matrices corresponding
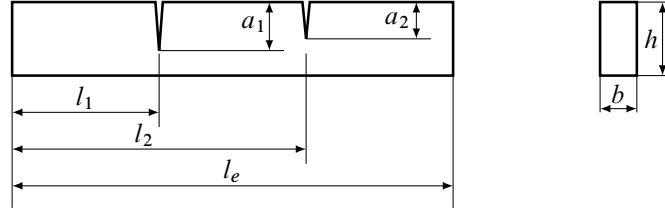
Figure 3. Beam element with two cracks.

to the mechanical coupling, electromechanical coupling, and electrical degrees of freedom, respectively. $\{F^e\}$ and $\{Q^e\}$ are the mechanical and electrical charge load vectors, respectively. The size of the element matrices are $[4 \times 4]$ and are given by

$$[M_{ww}^e] = \int_V [N_w]^T \rho [N_w] \, dV, \quad [K_{ww}^e] = \int_V [B_w]^T \hat{C} [B_w] \, dV,$$

$$[K_{w\phi}^e] = \int_V [B_w]^T \hat{e} [B_\phi] \, dV, \quad [K_{\phi\phi}^e] = \int_V [B_\phi]^T \hat{\epsilon} [B_\phi] \, dV. \tag{11}$$

In order to solve this, the global matrix equation (10) can be expanded and written as

$$[M_{ww}]\{\ddot{w}\} + [C_{ww}]\{\dot{w}\} + [K_{ww}]\{w\} + [K_{w\phi}]\{\phi\} = \{F\},$$

$$[K_{w\phi}]^T \{w\} + [K_{\phi\phi}]\{\phi\} = \{Q\}. \tag{12}$$

The second part of (12) is simplified as

$$\{\phi\} = [K_{\phi\phi}]^{-1}\{Q\} - [K_{\phi\phi}]^{-1}[K_{w\phi}]^T \{w\}. \tag{13}$$

The above equation is substituted in the first part of (12) and is written as

$$[M_{ww}]\{\ddot{w}\} + [C_{ww}]\{\dot{w}\} + [K_{ww}]^*\{w\} = \{F\}^*, \tag{14}$$

where

$$[K_{ww}]^* = [K_{ww}] - [K_{w\phi}][K_{\phi\phi}][K_{w\phi}]^T,$$

$$\{F\}^* = \{F\} - [K_{w\phi}][K_{\phi\phi}]^{-1}\{Q\}. \tag{15}$$

For the sensor problem, displacement histories are obtained by solving (14), and by substituting into (13), the voltage vector across the sensor patch is obtained.

5. FEM formulation of beam element with multiple cracks

5.1. *Double crack per beam element model.* The finite element formulation of the double crack per element model is explained here and it is identified as two cracks per beam element. This has hitherto not been incorporated in a one-dimensional PZT patch model, and also its application in an inverse problem of crack identification is novel. The crack per beam element and corresponding finite element model are shown in Figures 3 and 4 respectively. Let l_e be the length of the element, l_1 and l_2 are the locations of the crack from its left end, a_1 and a_2 respectively are the crack depths measured from the top of the beam.
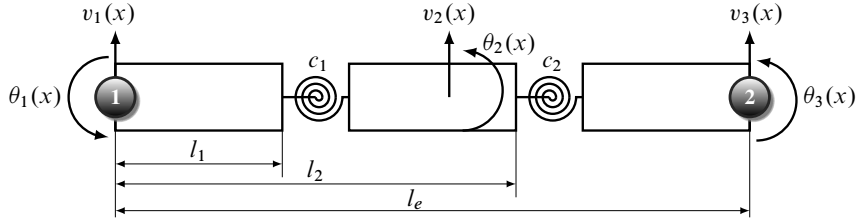
Figure 4. Equivalent model of cracked beam element.

The finite element model of two cracks per beam element contains three segments connected by two massless hinges of flexibility c_1 and c_2, respectively, as shown in Figure 4. Three different polynomials are assumed for the field variables of this element since it has three different segments:

$$
\left.
\begin{aligned}
v_1(x) &= b_1 + b_2 x + b_3 x^2 + b_4 x^3 \\
\theta_1(x) &= v_1'(x) = b_2 + 2b_3 x + 3b_4 x^2
\end{aligned}
\right\} \quad 0 \le x \le l_1;
$$

$$
\left.
\begin{aligned}
v_2(x) &= b_5 + b_6 x + b_7 x^2 + b_8 x^3 \\
\theta_2(x) &= v_2'(x) = b_6 + 2b_7 x + 3b_8 x^2
\end{aligned}
\right\} \quad l_1 \le x \le l_2; \tag{16}
$$

$$
\left.
\begin{aligned}
v_3(x) &= b_9 + b_{10} x + b_{11} x^2 + b_{12} x^3 \\
\theta_3(x) &= v_3'(x) = b_{10} + 2b_{11} x + 3b_{12} x^2
\end{aligned}
\right\} \quad l_2 \le x \le l_e;
$$

where b_1–b_{12} are the polynomial constants. The following are the nodal values and conditions applied to the cracked beam element:

$$
\begin{aligned}
v_1(0) &= Y_1, \quad \theta_1(0) = \Theta_1, \quad v_3(l_e) = Y_2, \quad \theta_3(l_e) = \Theta_2, \\
v_1(l_1) &= v_2(l_1), \quad v_1''(l_1) = v_2''(l_1), \quad v_1'''(l_1) = v_2'''(l_1), \\
v_2(l_2) &= v_3(l_2), \quad v_2''(l_2) = v_3''(l_2), \quad v_2'''(l_2) = v_3'''(l_2), \\
v_2''(l_1) &= \frac{1}{Kc_1}(\theta_2(l_1) - \theta_1(l_1)), \quad v_3''(l_2) = \frac{1}{Kc_2}(\theta_3(l_2) - \theta_2(l_2)).
\end{aligned}
$$

The flexibility coefficients $K_{c_1} = EIc_1$ and $K_{c_2} = EIc_2$ at crack locations. EI is the flexural stiffness and c is the torsional flexibility of the crack; Y_1, Θ_1, Y_2, and Θ_2 are the displacement and rotation at the nodes 1 and 2 respectively. The flexibility coefficient at the crack location can be also expressed as [Viola et al. 2001]

$$
K_{c1,c2} = h f(\xi)/2, \tag{17}
$$

where $f(\xi)$ is a correction function which takes into account the body and crack geometry and depends on the dimensionless crack ratio $\xi_{1,2} = a_{1,2}/h$ which can be represented as follows [Viola et al. 2001]:

$$
f(\xi) = \xi^2 \big(12 - 19.5\xi + 70.1\xi^2 - 97.6\xi^3 + 142\xi^4 - 138\xi^5 + 128\xi^6 - 132\xi^7
$$
$$
+ 379\xi^8 - 417\xi^9 + 131\xi^{10} + 313\xi^{12} - 357\xi^{13} + 102\xi^{14}\big), \quad 0 \le \xi < 0.5;
$$

$$
f(\xi) = \frac{1.32}{(1 - \xi^2)} - 1.78, \quad 0.5 \le \xi \le 1. \tag{18}
$$

The shape function matrix $[N(x)]$ of size 6×4 relates the nodal DOF with the field variables as follows:

$$
\begin{Bmatrix} v_1(x) \\ \theta_1(x) \\ v_2(x) \\ \theta_2(x) \\ v_3(x) \\ \theta_3(x) \end{Bmatrix} = \begin{bmatrix} N_{11}(x) & N_{12}(x) & N_{13}(x) & N_{14}(x) \\ N_{21}(x) & N_{22}(x) & N_{23}(x) & N_{24}(x) \\ N_{31}(x) & N_{32}(x) & N_{33}(x) & N_{34}(x) \\ N_{41}(x) & N_{42}(x) & N_{43}(x) & N_{44}(x) \\ N_{51}(x) & N_{52}(x) & N_{53}(x) & N_{54}(x) \\ N_{61}(x) & N_{62}(x) & N_{63}(x) & N_{64}(x) \end{bmatrix} \begin{Bmatrix} Y_1 \\ \Theta_1 \\ Y_2 \\ \Theta_2 \end{Bmatrix}. \tag{19}
$$

From the finite element procedure, the stiffness and mass matrices of the cracked element can be obtained as

$$
[k_{cr}^e] = EI \left(\int_0^{l_1} B_1^T B_1 \, dx + \int_{l_1}^{l_2} B_2^T B_2 \, dx + \int_{l_2}^{l_e} B_3^T B_3 \, dx \right), \tag{20}
$$

$$
[m_{cr}^e] = \rho A \left(\int_0^{l_1} N_1(x)^T N_1(x) \, dx + \int_{l_1}^{l_2} N_3(x)^T N_3(x) \, dx + \int_{l_2}^{l_e} N_5(x)^T N_5(x) \, dx \right). \tag{21}
$$

where $B_1 = d^2[N_1(x)]/dx^2$, $B_2 = d^2[N_3(x)]/dx^2$, and $B_3 = d^2[N_5(x)]/dx^2$. Here, $N_1(x)$, $N_2(x)$, $N_3(x)$, $N_4(x)$, $N_5(x)$, and $N_6(x)$ are the respective rows of the shape function matrix $N(x)$. Since the effect of rotation of the beam element is very small when compared with translation of beam, it may be neglected. This can be extended to any number of cracks per element. When either Kc_1 or Kc_2 is zero, the element becomes a single crack per element model as in previous literature [Krawczuk et al. 2000; Viola et al. 2001]. The single crack per element with one-dimensional PZT patch in structural identification (SI) has not yet been reported. When the values of $Kc_1 = Kc_2 = 0$, the structure is considered as an intact element.

6. Particle swarm optimization (PSO) algorithm

A heuristic optimization technique referred to as particle swarm optimization PSO is used here which mimics the social behavior of swarms. It was first proposed by James and Eberhart [Kennedy and Eberhart 1995]. Heuristic methods are preferred over calculus-based methods due to their robustness and ability to attain the global optima. It imitates the social behavior of a swarm of birds. Each bird tends to follow the general swarm direction in search of the target (food), but it has a component of its own intelligence and memory (i.e., local search) which influences its action. Each bird is visualized as a "particle" which approaches the target (i.e., the global optima) with a "velocity". The number of particles (i.e., population) and their initial random positions are specified. As the particles progress to the global optima through many generations, their current position is updated using two parameters: G_{best}, which represent the historically best coordinate of all the particles in the population, and $P_{\text{best},i}$, the historically best coordinate of the i-th particle. The equations giving the velocity v and position x for the i-th particle in the $k + 1$ generation are given by

$$
v_i(k+1) = \varphi(k)v_i(k) + \alpha_1[\gamma_{1i}(P_{\text{best},i} - x_i(k))] + \alpha_2[\gamma_{2i}[(G_{\text{best}} - x_i(k))], \tag{22}
$$

$$
x_i(k+1) = x_i(k) + v_i(k+1), \tag{23}
$$

where i is the particle index, k the discrete time index, v the velocity of the i-th particle, and x the position of the i-th particle in the present solution. Here, γ_1 and γ_2 represent two random numbers between zero

and one, φ is an inertia term uniformly decreasing from 0.9 to 0.4 with passing generations, and α_1 and α_2 are two acceleration constants set to two [Perez and Behdinan 2007]. Several studies have pointed out the superiority of the PSO algorithm over the more conventional heuristic algorithms such as the genetic algorithm (GA) for inverse problem applications [Mohan et al. 2014; Mouser and Dunn 2005].

7. Crack identification using one-dimensional PZT patch

In the proposed method, a patch is attached to either end of the beam member whose crack parameters have to be identified. The time-domain-based approach is used and the voltage history of the patch is used as the main response quantity in the identification of structural stiffness and crack parameters. A few experimentally measured voltage potential responses ϕ^m are measured from PZT patches. The estimated voltage potential ϕ^e is obtained from the mathematical model using (13). For exact identification, ϕ^e has to match with the experimentally measured responses ϕ^m. In this method, experimental responses are simulated from a known numerical model and polluted with Gaussian noise of zero mean and a certain standard deviation. Using the particle swarm optimization (PSO) algorithm, the following fitness (objective) function is minimized, which is the sum of squares of deviations between the measured and estimated voltage. The fitness or objective function is

$$f = \frac{\sum_{i=1}^{M} \sum_{j=1}^{L} |\phi^m(i, j) - \phi^e(i, j)|^2}{ML}. \tag{24}$$

The superscripts m and e denote measured and estimated responses for fitness evaluation, M is the number of measurement sensors used, and L is the number of time steps. Ideally, it must be minimized to zero, but usually it approaches a value close to zero. The minimization of the fitness function gives the identified crack depth and location variables.

8. Numerical examples and results

Here, three different types of numerical studies are carried out for validating the proposed identification method. A fixed-fixed beam with two cracks (assuming a single crack per element), the same beam with four cracks, and substructures (SS) of the frame structure with nine members and four cracks (assuming two cracks per element). A patch is attached to either end of the beam member. The structural parameters, such as mass and stiffness of the undamaged structure, are assumed to be known. Experimental measured responses are numerically simulated from a fully defined model in MATLAB using Newmark's constant acceleration scheme. The structure is excited by an impulse or harmonic force and the corresponding voltage responses are measured at the PZT patches. The crack parameters such as location and depth are estimated using the inverse formulation with a single objective approach. In order to simulate the effect of noise in experiments, a Gaussian random noise level of 5% (standard deviation) and zero mean is added to all the measured signals. The noise is added with simulated responses in such a way that

$$\text{Noise} = g \times \text{RMS}_{\text{signal}} \times NL \tag{25}$$

where g is the standard Gaussian variable, $\text{RMS}_{\text{signal}}$ is the root mean square (RMS) value of the numerically simulated signal, and NL is noise level.
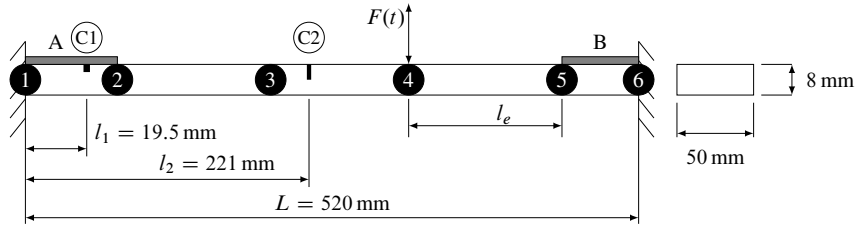
Figure 5. Finite element model of two single cracks per beam element with PZT patch.

In this numerical study, three different PZT patch lengths are investigated, and they are PZT : 5%, PZT : 10%, and PZT : 20%. They respectively represent the length of the patch expressed as percentage of beam length. The width of PZT is the same as the host structure and a constant thickness of 1 mm is used for this study.

8.1. *Example 1: fixed-fixed beam with multiple cracks using single crack per element.* The crack detection by the proposed method is applied on the fixed-fixed beam structure to determine the magnitude (crack depth) and locations of two cracks simultaneously. The same cracked steel beam was studied in [Verhese and Shankar 2014; Viola et al. 2001]: it is 520 mm long, 50 mm wide, and 8 mm thick with a Young's modulus (E) of 206 GPa and density of 7850 kg/m^3. The two open edge cracks are assumed to be located at 19.5 mm and 221 mm from the left end of beam, respectively, and it is also assumed that the cracks in different elements do not interact with each other. The absolute normalized crack location measured from the left end of the beam are $\lambda_{C1}(l_1/L) = 0.0375$ and $\lambda_{C2}(l_2/L) = 0.425$. Crack depths of 0.4 mm and 4 mm are considered and the corresponding normalized crack depths are $\xi_{C1}(a/h) = 0.05$ and $\xi_{C2}(a/h) = 0.5$ respectively. The beam is divided into five Euler finite elements as shown in Figure 5 and cracks lie in the first and third elements. It may be noted that the first crack is located under the PZT patch.

In this study, as in the first case, two PZT patches with size PZT : 5%, i.e., ($26 \times 50 \times 1$ mm^3 PZT) is bonded on either end of the structure as shown in Figure 5. The first and second natural frequency of the modes of vibration of the cracked structure are 151.29 Hz and 430.97 Hz respectively. Rayleigh damping with a modal damping ratio of 3% is used for the first two modes of vibration. The beam is subjected to a harmonic excitation of $F(t) = 2.5 \sin(2\pi 130t)$ N in the vertical (upward) direction at node 4. The displacement, velocity, and acceleration time history data are calculated for each nodal point using Newmark's method with a constant time step of 0.001 s. Using the displacement response history, voltage responses are measured through two PZT patches. Figure 6 shows the undamaged and damaged responses available at the measurement PZT patch sensor A for multiple crack locations. The shift in damaged response for multiple cracks is greater than a single crack. The numerically calculated voltages are polluted by artificially adding Gaussian white noise with zero mean and a standard deviation of 5% to simulate experimental errors.

The mass and intact stiffness EI of the structure are assumed to be known a priori. The proposed algorithm identifies multiple cracks assuming that each element contains a single crack. The normalized crack location in element 1 with respect to left end of the element is $\lambda_{e1} = 0.75$ and the same in element 3 is $\lambda_{e3} = 0.25$. Here, crack magnitude and location are set as the unknown variables for each element and
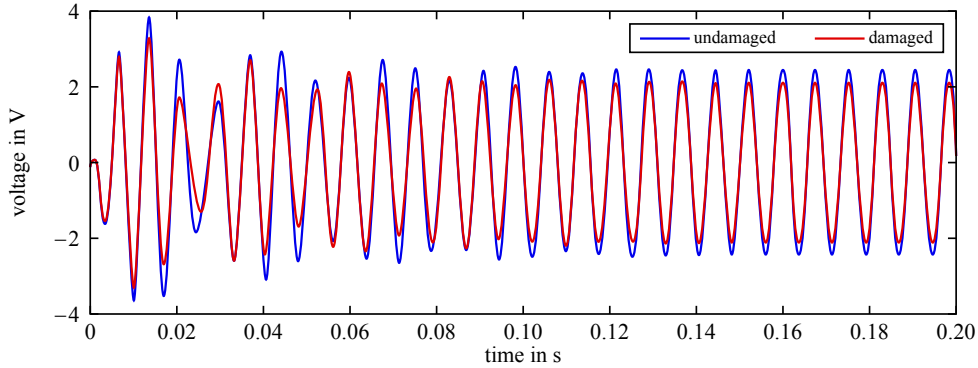
Figure 6. Harmonic response at measurement (PZT A) with multiple crack locations.

patch length	crack depth ξ (exact)	crack location λ (exact)	crack depth ξ (identified)		crack location λ (identified)	
			noise-free (% error)	5% noise (% error)	noise-free (% error)	5% noise (% error)
PZT: 5%	0.05 (C1)	0.0375	0.0478 (4.4)	0.0535 (7)	0.0382 (−1.87)	0.0385 (−2.67)
	0.5 (C2)	0.425	0.4967 (0.66)	0.5062 (−1.24)	0.4245 (−0.12)	0.4298 (−1.13)
PZT: 10%	0.05 (C1)	0.0375	0.0519 (−3.8)	0.0469 (6.2)	0.0369 (1.6)	0.0383 (−2.13)
	0.5 (C2)	0.425	0.5031 (−0.62)	0.4951 (1.18)	0.4255 (0.12)	0.4208 (0.99)
PZT: 20%	0.05 (C1)	0.0375	0.0483 (3.4)	0.0529 (−5.8)	−0.0380 (1.33)	0.0368 (1.87)
	0.5 (C2)	0.425	0.4978 (0.44)	0.5055 (−1.1)	0.4253 (−0.07)	0.4292 (0.96)

Table 2. Crack damage magnitude and location with voltage matching. All values are normalized.

hence there are ten unknown variables in this problem. Thus the optimization variables to be identified are the normalized crack depth ξ and normalized location $\lambda_e = l_1/l_e$ in five elements. The experimentally measured voltage response of PZT patches is required for the fitness evaluation. The mean square error (MSE) between measured and predicted voltage response at PZT patches are minimized by particle swarm optimization. The lower and upper bounds for PSO optimization for identifying crack magnitude are set at zero and one. Similarly the lower and upper bounds to identify normalized crack locations are set as zero and l_e, respectively. Here, PSO parameters are set to 100 particles (swarm size) and 500 generations. Similar numerical studies are carried out with larger patch lengths, such as PZT: 10%, i.e., $(52 \times 50 \times 1 \, \text{mm}^3 \, \text{PZT})$ and PZT: 20%, i.e., $(104 \times 50 \times 1 \, \text{mm}^3 \, \text{PZT})$. The crack depth and location are estimated using different sets of iterations and the mean identified crack parameters are presented in Table 2.

The smallest crack depth $\xi = 0.05$ located under the PZT patch is identified with an absolute error of 7%, 6.2%, and 5.8%, respectively for PZT: 5%, PZT: 10%, and PZT: 20% with noisy condition. From Table 2, it can be seen that crack location identification is better than crack depth estimation. Here, the smallest patch length (PZT: 5%) identified the crack location with an absolute error of 2.67% under the noisy condition. The element-wise details of crack depth identification using different patch lengths are shown in Figure 7 for the noise-free and noisy cases. Figure 8 shows the comparison of convergence
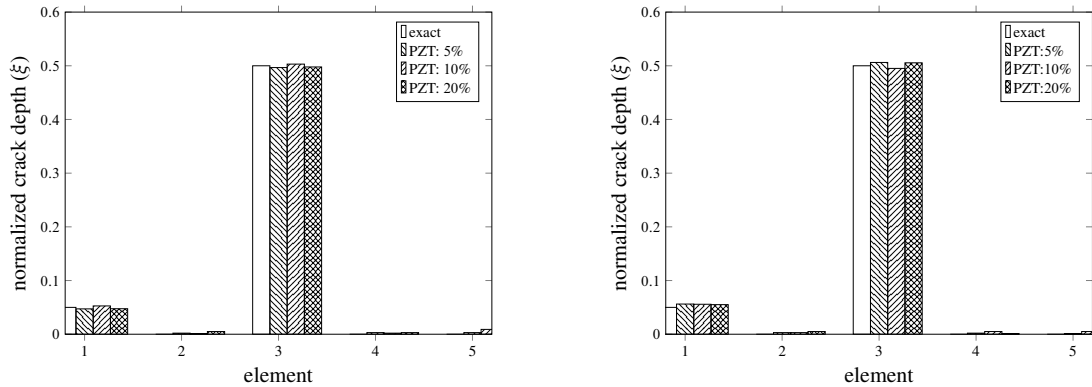
Figure 7. Normalized damage magnitude of multiple cracks. Left: noise-free case. Right: 5% noise case.
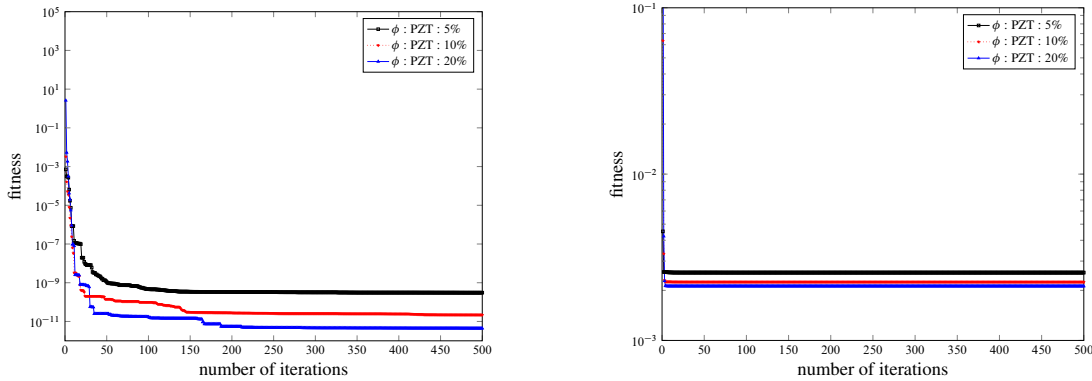

Figure 8. Convergence plot for $\xi = 0.05$. Left: noise-free case. Right: 5% noise case.

studies of different PZT patch lengths. Here, the objective function of PZT: 20% has minimized better than smaller patch lengths and is most accurate in identification. However, it is not required to use such a large patch length. As compared to PZT: 5%, the percentage decrease of error by PZT: 20% is only 8–15%. Thus for practical and economical aspects, PZT: 5% is sufficient for estimating crack parameters.

Now, the proposed method is compared with similar existing published results. Viola et al. [2002] identified the crack depth $\xi = 0.5$ and location $\lambda = 0.76$ based on the modal approach using experimentally measured results. The identified crack parameters are 0.486 and 0.756 and the percentage of the absolute error is 2.8% and 0.53% respectively for crack depth and location. It may be noted that here only a single crack is identified. The very same multicrack problem of similar crack depth $\xi = 0.5$ was solved by Verhese and Shankar [2014] using a combined transient power flow and acceleration matching technique with a substructure approach. There, normalized crack depth and location of the same crack depth were identified with absolute errors of 3.26%, 4.04%, and 1.59%, 2.98% respectively for the noise-free and 5% noisy cases. The proposed method using PZT : 5% estimated the crack depth and location of a similar crack with errors of 0.66%, 1.24%, and 0.117%, 1.13%, respectively for the noise-free and noisy cases. Here, mean computational time is only about 140 s whereas in the other study it was 3000 s.
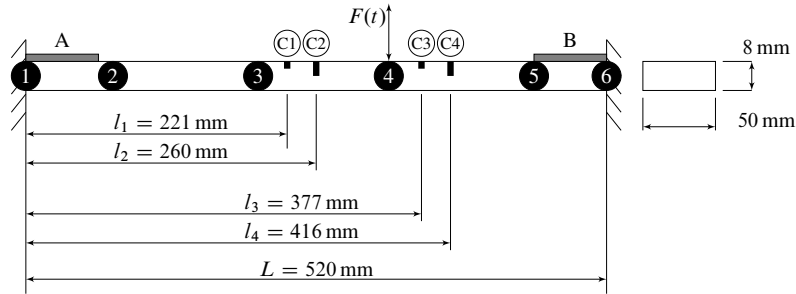
Figure 9. Finite element model of two double cracks per beam element with PZT patch.
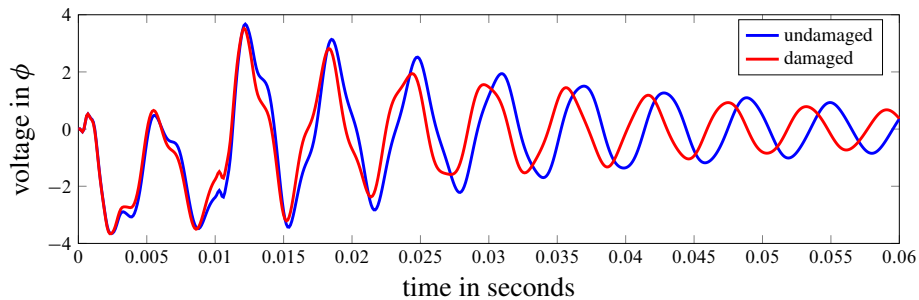
Figure 10. Impulse response at measurement (PZT A) with multiple double crack locations.

8.2. *Example 2: fixed-fixed beam with two double crack per element.* The same beam in Section 8.1 is considered for the crack identification with a double crack per beam element. Here, four open edge cracks of depths 0.4 mm, 4 mm, 0.8 mm, and 2 mm are assumed to be located at a distances of 221 mm, 260 mm, 377 mm, and 416 mm respectively from the fixed end. In this study, the beam is divided into five elements; two open edge cracks C_1, C_2 are placed in element 3, and C_3, C_4 are placed in element 4, as shown in Figure 9. It is assumed that cracks are not interacting with each other. The normalized crack depths ($\xi = a/h$) are $\xi_{C1} = 0.05$, $\xi_{C2} = 0.5$, $\xi_{C3} = 0.1$, and $\xi_{C4} = 0.25$ and the corresponding absolute crack locations are $\lambda_{C1} = 0.425$, $\lambda_{C2} = 0.5$, $\lambda_{C3} = 0.725$, and $\lambda_{C4} = 0.8$.

In this study, PZT: 5% and PZT: 10% are used for the crack parameter estimation. As in the first case, two PZT patches of size PZT: 5% are bonded on either side of the structure as shown in Figure 9. Here, the normalized crack locations in the element 3 with respect to left end of the element are $\lambda_{e31} = 0.25$ and $\lambda_{e32} = 0.5$, and the same in the element 4 are $\lambda_{e41} = 0.25$ and $\lambda_{e42} = 0.5$. (Here, λ_{e31} represents crack 1 in element 3, i.e., C_1.)

The fundamental natural frequency of the cracked structure is 150.87 Hz. Rayleigh damping with the modal damping ratio of 3% is used for the first two modes of vibration. The beam is excited by providing an impulse force of 5 N at node 4 over a time of 0.01 s in a time step of 0.001 s and a voltage response is measured through PZT patches. Figure 10 shows the comparison between the damaged and undamaged response of the beam at the PZT patch A and the change in dynamic response is greater than a single crack.

identified crack depth (noise-free)   identified crack location (noise-free)

identified crack depth (5% noise)   identified crack location (5% noise)
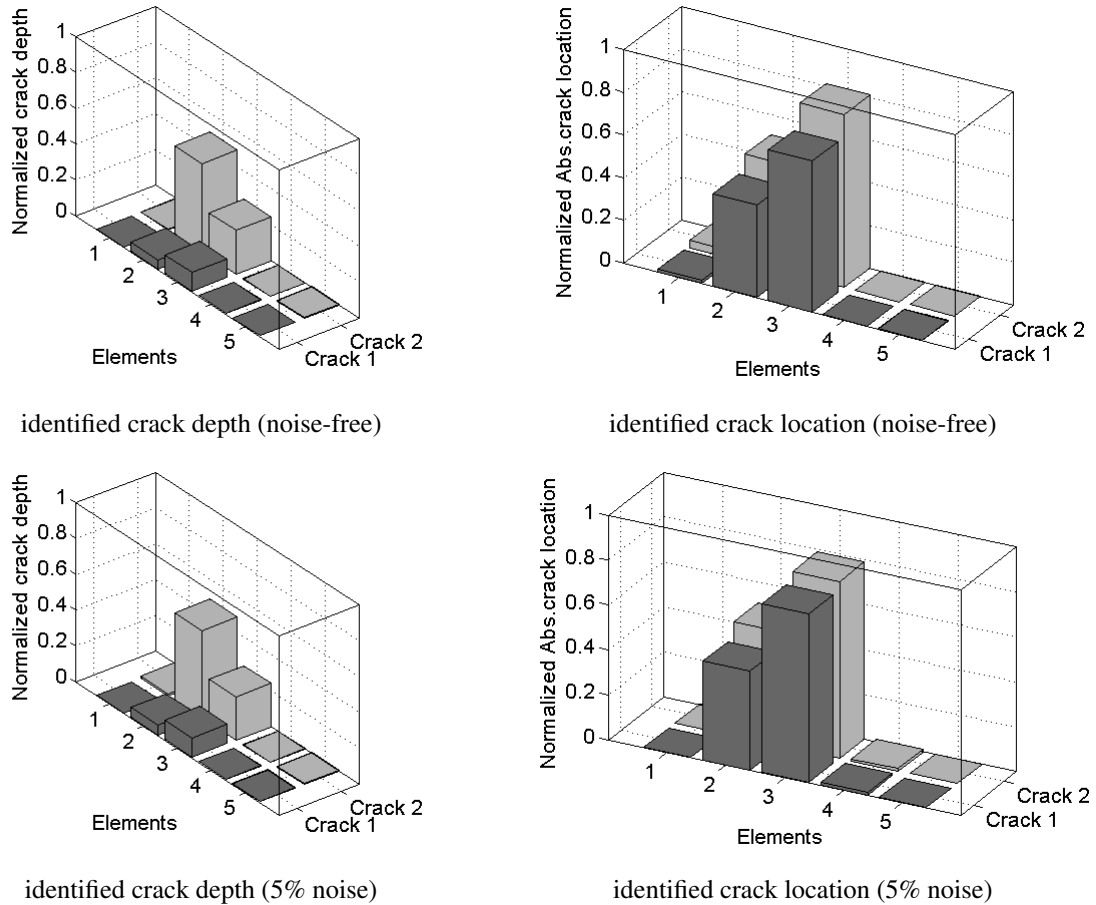
Figure 11. Identified crack parameters of fixed-fixed beam with PZT: 5%.

Here, for crack parameter estimation, it is assumed that each finite element of the model contains two cracks at different positions. Crack magnitude and location are unknown variables and thus each element contains four unknown variables. Hence, a total of twenty variables are searched between the value of zero to one by PSO. The MSE between the measured and predicted voltage responses is minimized by PSO with a swarm size of 100 and with 500 iterations. The identified parameters with PZT: 5% is shown in Figure 11 and the percentage of absolute error of identified parameters of each crack is shown in Figure 12. The smallest crack of depth ($\xi = 0.05$) is identified with an absolute error of 4.89% for noise-free measurement and 9.05% with 5% noise level measurement. The normalized location of the same crack is identified with an error of 1.76% without noise and 3.36% with 5% noise in measurements.

The numerical study was carried out for PZT: 10% with similar crack depth and location for the same beam. Figure 13 shows the comparison of convergence of fitness (objective) functions for PZT: 5% and PZT: 10% for four cracks (noise-free and noisy case), respectively. The better minimization of PZT: 10% when compared with PZT: 5% is seen from the plot. Hence, the error of both magnitude and location is reduced. The identified parameters are shown in Figure 14 and absolute errors in those parameters are
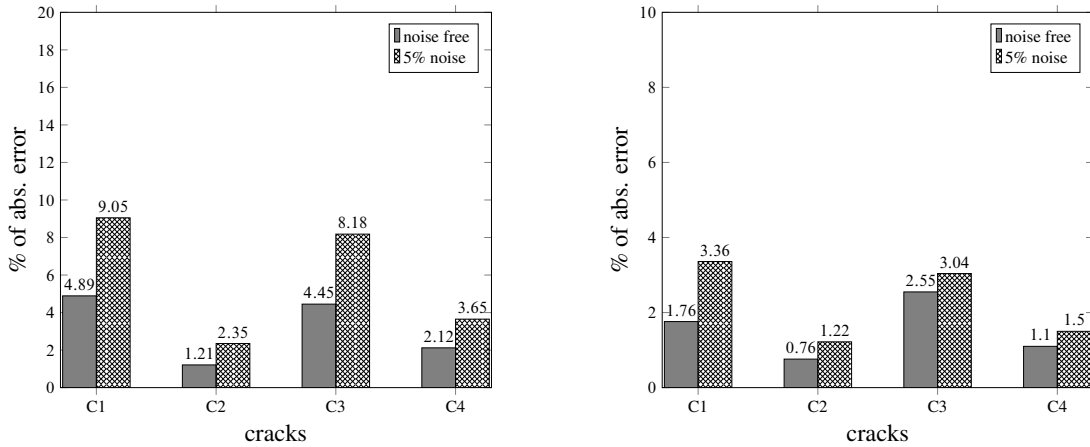
Figure 12. Absolute error in identified parameters in fixed-fixed beam with PZT: 5%. Left: depth. Right: location.
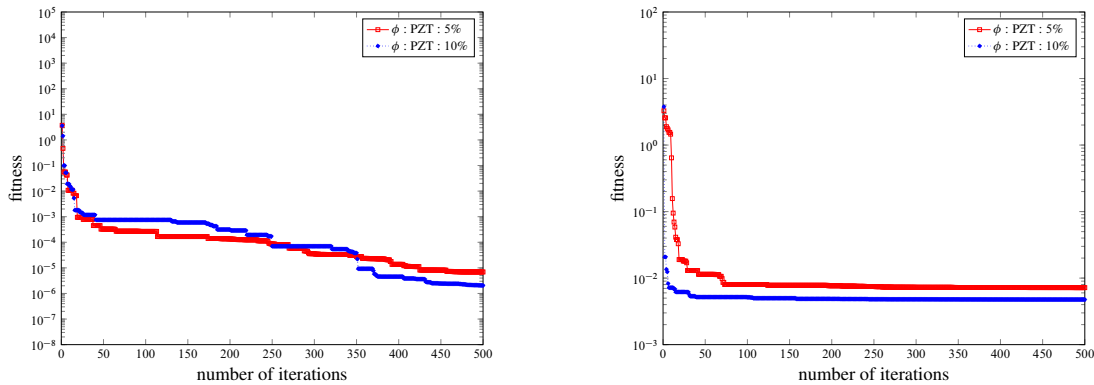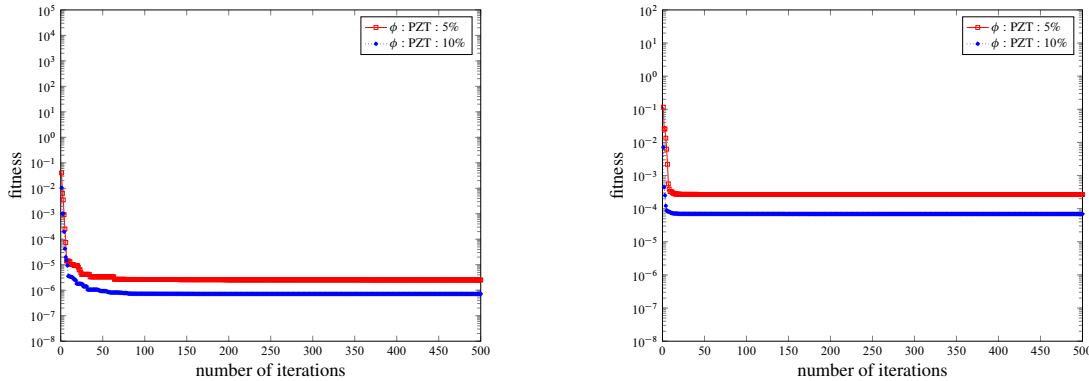

Figure 13. Convergence plot for multiple cracks with two double-cracks per beam element. Left: noise-free case. Right: 5% noise case.

shown in Figure 15. In this case, the smallest crack depth ($\xi = 0.05$) is identified with an absolute error of 4.03% with noise-free measurement and 8.75% with 5% noise level measurement. The error in its location is 1.5% without noise and 3.21% with 5% noise. Here, due to an increase in sensitivity, it can be observed that there is an improvement in identification of smaller crack depth and location. It is also seen that both patch lengths identified the location more accurately than crack depth.

8.3. *Example 3: substructure* (SS) *of frame with double crack per beam element.* In this example, a steel frame structure consisting of nine members is fixed at two supports, as shown in Figure 16 as per [Nandakumar and Shankar 2014]. The density of the frame material is 7850 kg/m^3 and its Young's modulus (E) is 200 GPa. Each member has a flexural rigidity (EI) of 43.2 N · m^2, and a cross-section of 12 × 6 mm. Four open edge cracks of depth 0.3 mm, 1.5 mm, 3 mm, and 2 mm are considered at a distances of 200 mm, 275 mm, 725 mm, and 800 mm respectively from the left end of member 4, as shown in Figure 16. The fundamental natural frequency of the cracked structure is 11.9 Hz. The normalized

identified crack depth (noise-free)

identified crack depth (noise-free)

identified crack depth (5% noise)

identified crack location (5% noise)
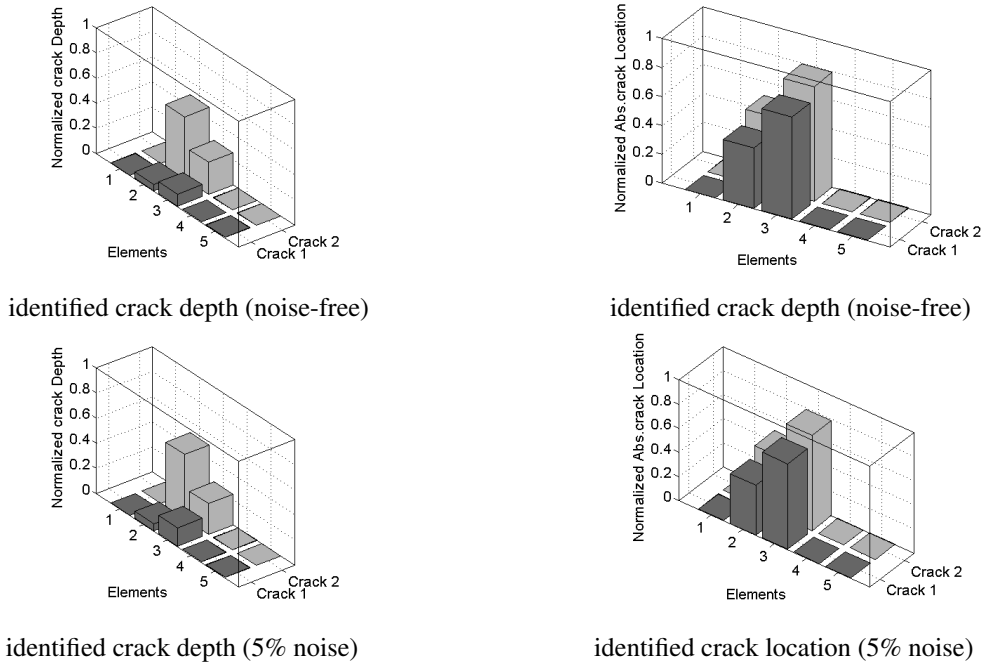
Figure 14. Identified crack parameters of fixed-fixed beam with PZT: 10%.
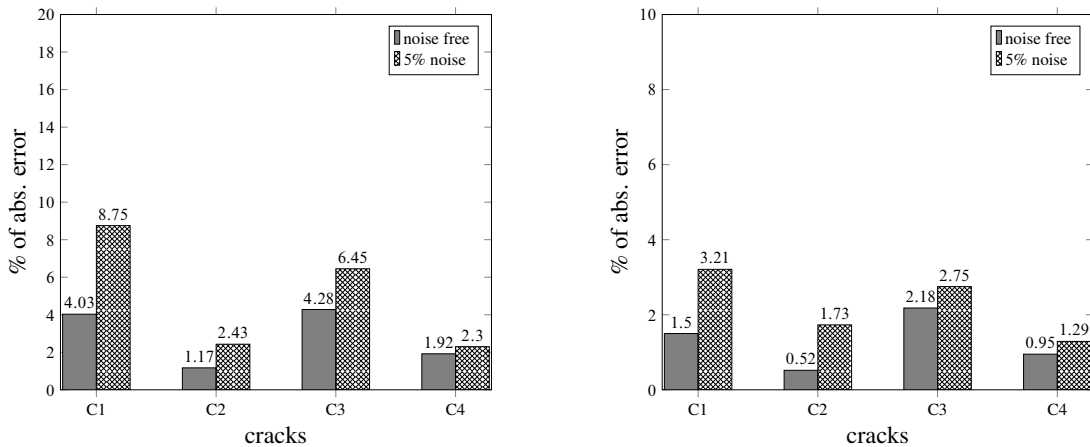
Figure 15. Absolute error in identified parameters in fixed-fixed beam with PZT: 10%.
Left: depth. Right: location.

crack depths for the above cracks are $\xi_{c1} = 0.05$, $\xi_{c2} = 0.25$, $\xi_{c3} = 0.5$, and $\xi_{c4} = 0.33$ and their absolute normalized locations from the left end of member 4 are $\lambda_{c1} = 0.2$, $\lambda_{c2} = 0.275$, $\lambda_{c3} = 0.725$, and $\lambda_{c4} = 0.8$. It is proposed to detect the cracks locally in the SS (member 4) of the frame using PZT : 5%, which is shown inside the dotted box in Figure 16, left.
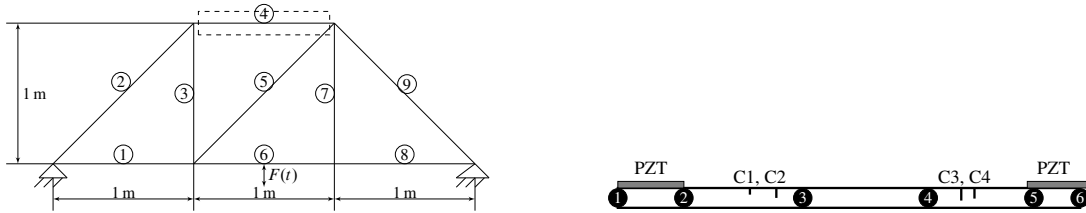
Figure 16. Frame structure. Left: global structure. Right: substructure of member four with six nodes.

Figure 17. Convergence plot for multiple cracks with two double-cracks per beam element. Left: noise-free case. Right: 5% noise case.

The damping effect in the structure is modeled using Rayleigh's damping model, with a damping ratio of 3%. The structure is excited by an impulse response of 10 N over a time of 0.01 s, with a time step of 0.001 s, at the midpoint of member 6. Frame member 4 is divided into five elements as shown in Figure 16, right; the first two cracks lie on the element 2 and the remaining two cracks lie on the element 4. The normalized locations from the left end of the respective elements are $\lambda_{e2.1} = 0.5$, $\lambda_{e2.2} = 0.75$, $\lambda_{e4.1} = 0.25$, and $\lambda_{e4.2} = 0.5$ ($\lambda_{e2.1}$ means that crack 1 is in the element 2). The crack parameters are searched by PSO with swarm size 100 and 500 generations, as explained in the previous example. The identified parameters of absolute error are shown in Figure 18. The crack with smallest depth ($\xi = 0.05$) is identified with an absolute error of 5.3% without noise and 12.97% with 5% noise in measurement. The location of this crack is identified with an absolute error of 2.52% and 4.05% without and with 5% noise in measurement, respectively. The total time taken for the convergence is 215 s.

9. Experimental verification: fixed-fixed beam with PZT patches

A fixed-fixed beam made of acrylic material with dimensions 452 mm × 25 mm × 12 mm is used for the experimental study. Here two PZT patch of dimensions 25 mm × 25 mm × 1 mm each are bonded at the fixed ends of the structure as shown in Figure 19. The modulus of elasticity (E) was estimated to be 3.9 GPa from a simple bending test and the density was measured to be 1190 kg/m^3. The actual flexural rigidity (EI) of the beam is 14.04 N · m^2. The damping ratio (ζ) was calculated from a simple free
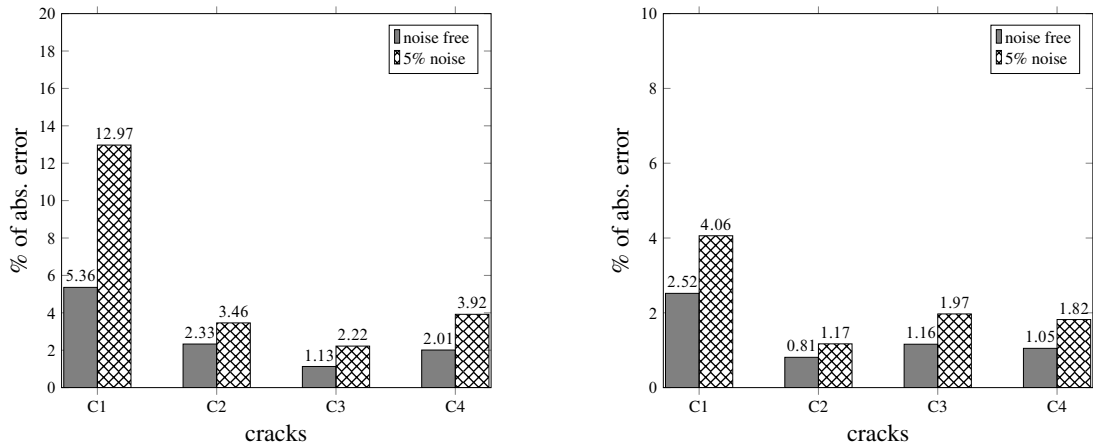
Figure 18. Absolute error in identified parameters in SS of frame with PZT: 5%. Left: depth. Right: location.
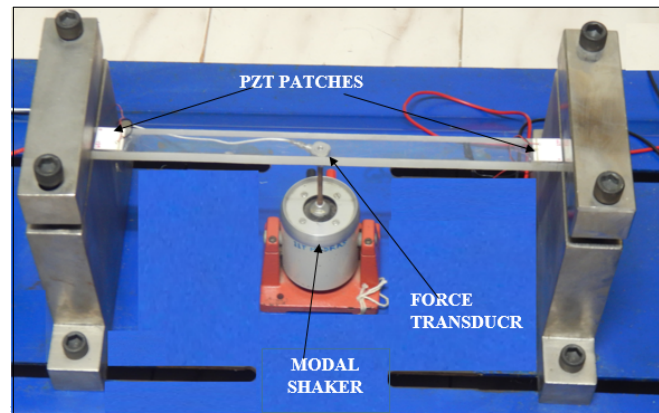

Figure 19. Experimental set up of fixed-fixed intact beam with PZT patch.

vibration decay test using logarithmic decrement and was estimated as 8%. The natural frequencies for the first two modes of the structure were calculated from the frequency domain as 110 Hz and 306 Hz.

The beam is excited by a sinusoidal force of $2.2 \sin(2\pi \times 68.3t)$ N at the middle of the structure by a LDS permanent magnet 20 N modal shaker with a maximum displacement of 5 mm with an operating frequency range of 5 Hz–13 kHz. The applied force is measured by using a KISTLER force transducer and is acquired with a sampling frequency of 1000 Hz using a DEWE 43 DAQ system. The dynamic voltage response is measured through two piezoelectric patches and it is sampled at a rate of 1000 Hz. The comparison of experimental and simulated voltage response (time and frequency domain) of the given intact beam is shown in Figure 20. One can find that difference in measured and calculated response is very small, which shows the one-dimensional (1-D) hybrid model is accurate.

Next, two open edge cracks of depths 6 mm and 1.5 mm are introduced on the same beam at a distances of 92 mm and 393.5 mm from the fixed end. The width of cut is 0.4 mm and close-up views of the cracks
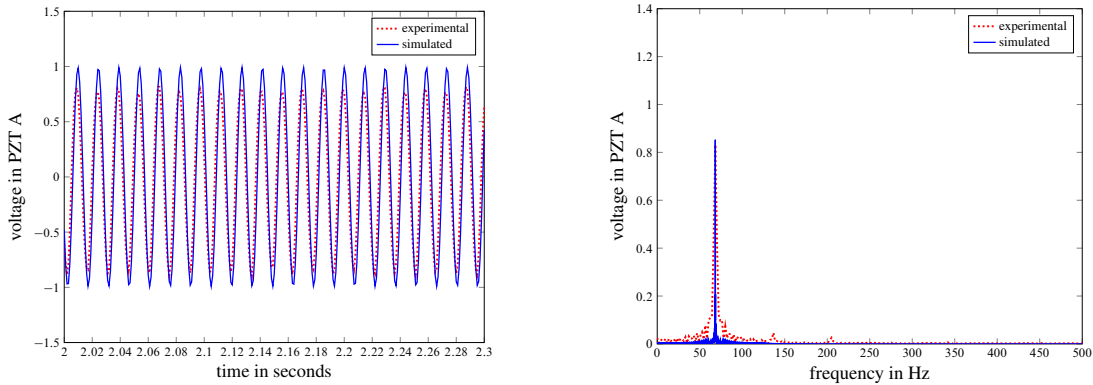
Figure 20. Experimental and simulated voltage response at PZT A. Left: time domain. Right: frequency domain.
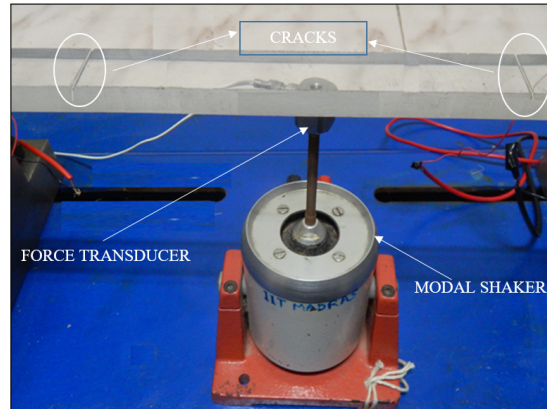
Figure 21. Cracks in the fixed-fixed beam.

are shown in Figure 21. The nondimensional crack depth of each crack is $\xi_1 = 0.5$ and $\xi_2 = 0.125$, and their absolute location from the fixed end are $\lambda_1 = 0.2$ and $\lambda_2 = 0.87$, respectively. The beam is divided into five elements as in the previous numerical study, and here, the crack lies in the second and fourth elements, respectively. The nondimensional element-wise crack locations measured from the left node of the element are $\lambda_{e2} = 0.5$ and $\lambda_{e4} = 0.75$, respectively. The cracked structure is excited by a harmonic force of $2.8 \sin(2\pi \times 60.7t)$ N at a distance of 292 mm from the left fixed end. The voltage responses are measured through the PZT patches and it is sampled at a rate of 1000 Hz. From the acquired data, a portion of time histories of 5 s is considered for parameter identification. The parameters are searched between the feasible search range of zero and one by PSO (swarm size: 200, generations: 500) using the proposed voltage matching technique. Damage parameters are identified from six different trials of reading and mean values are presented in Table 3. The smallest crack depth ($\xi = 0.125$) is identified with an absolute error of 12.56% in magnitude and 2.2% in its location. Similar to the numerical study, here identifying the crack location is more accurate than depth estimation.

exact crack depth ξ	exact absolute crack location λ	identified crack depth (% error)	identified crack location (% error)
0.5	0.2	0.5262 (-5.24)	0.1961 (1.95)
0.125	0.87	0.1093 (12.56)	0.8509 (2.2)

Table 3. Experimental identification (crack depth and location) of a multiple crack.

Now, the proposed method is compared with other similar experimental results in literature. Ding et al. [2017] estimated the crack parameters of two cracks (crack depth ratio $\xi = 0.1$) with crack locations ($\lambda_1 = 0.2$, $\lambda_2 = 0.45$) of a fixed-fixed beam using an improved artificial bee colony algorithm based on experimental frequency measurement data from [Khiem and Toan 2014]. There, the maximum identified crack depth and location error are 24% and 4% respectively. The proposed method has identified multiple cracks with a maximum absolute error of 12.56% and 2.2% respectively for crack and location.

10. Conclusions

This study presents a multiple crack detection scheme in beam structures by minimizing measured and predicted voltage responses of PZT patches. Unlike conventional accelerometer sensors, PZT patches have low cost and negligible weight, and a wide band width with the ability of dynamic measurement of distributed nature. A one-dimensional (1-D) hybrid beam element with a PZT sensor bonded to the beam represented by reduced material properties is used. Hitherto, the one-dimensional (1-D) patch with beam model was not used for structural identification, thereby unfolding a new model which is simple and convenient. The effect of different PZT lengths is investigated with numerical examples and the convergence of the fitness function of the cases are studied. Numerical examples show that the smallest patch length PZT: 5% (5% of the length of the beam) under study is sufficient enough for effective and accurate crack parameter identification. The proposed method estimated the crack depth error in the range of 0.66% to 12% and the location error in the range of 0.11% to 4% (noise-free and noisy case). The validation of the proposed method has also been carried out using experiments. The accuracy of the proposed method using the one-dimensional hybrid element model is found to be comparable or superior to some of the existing methods reviewed here.

References

[Bendary et al. 2010] I. M. Bendary, M. Adnan Elshafei, and A. M. Riad, "Finite element model of smart beams with distributed piezoelectric actuators", *J. Intell. Mater. Syst. Struct.* **21**:7 (2010), 747–758.

[Benjeddou 2000] A. Benjeddou, "Advances in piezoelectric finite element modeling of adaptive structural elements: a survey", *Compos. Struct.* **76**:1-3 (2000), 347–363.

[Ding et al. 2017] Z. Ding, Z. Lu, M. Huang, and J. Liu, "Improved artificial bee colony algorithm for crack identification in beam using natural frequencies only", *Inverse Probl. Sci. Eng.* **25**:2 (2017), 218–238.

[Douka et al. 2004] E. Douka, G. Bamnios, and A. Trochidis, "A method for determining the location and depth of cracks in double-cracked beams", *Appl. Acoust.* **65**:10 (2004), 997–1008.

[Fukunaga et al. 2002] H. Fukunaga, N. Hu, and F.-K. Chang, "Structural damage identification using piezoelectric sensors", *Int. J. Solids Struct.* **39**:2 (2002), 393–418.

[Kapuria and Hagedorn 2007] S. Kapuria and P. Hagedorn, "Unified efficient layerwise theory for smart beams with segmented extension/shear mode, piezoelectric actuators and sensors", *J. Mech. Mater. Struct.* **2**:7 (2007), 1267–1298.

[Kennedy and Eberhart 1995] J. Kennedy and R. Eberhart, "Particle swarm optimization", pp. 1942–1948 Proc. IEEE Int. Conf. Neural Netw. **1995**:4, IEEE, 1995.

[Khiem and Toan 2014] N. T. Khiem and L. K. Toan, "A novel method for crack detection in beam-like structures by measurements of natural frequencies", *J. Sound Vib.* **333**:18 (2014), 4084–4103.

[Krawczuk et al. 2000] M. Krawczuk, A. Żak, and W. Ostachowicz, "Elastic beam finite element with a transverse elasto-plastic crack", *Finite Elem. Anal. Des.* **34**:1 (2000), 61–73.

[Lee and Shin 2002] U. Lee and J. Shin, "A frequency-domain method of structural damage identification formulated from the dynamic stiffness equation of motion", *J. Sound Vib.* **257**:4 (2002), 615–634.

[Liu et al. 2011] H. Liu, K. Xin, and Q. Qi, "Study of structural damage detection with multi-objective function genetic algorithms", *Procedia Eng.* **12** (2011), 80–86.

[Mohan et al. 2014] S. C. Mohan, A. Yadav, D. K. Maiti, and D. Maity, "A comparative study on crack identification of structures from the changes in natural frequencies using GA and PSO", *Eng. Computation.* **31**:7 (2014), 1514–1531.

[Mouser and Dunn 2005] C. R. Mouser and S. A. Dunn, "Comparing genetic algorithms and particle swarm optimisation for an inverse problem exercise", *ANZIAM J.* **46** (2005), C89–C101.

[Nandakumar and Shankar 2014] P. Nandakumar and K. Shankar, "Multiple crack damage detection of structures using the two crack transfer matrix", *Struct. Health Monit.* **13**:5 (2014), 548–561.

[Patil and Maiti 2005] D. Patil and S. Maiti, "Experimental verification of a method of detection of multiple cracks in beams based on frequency measurements", *J. Sound Vibration* **281**:1 (2005), 439–451.

[Perez and Behdinan 2007] R. E. Perez and K. Behdinan, "Particle swarm approach for structural design optimization", *Comput. Struct.* **85**:19-20 (2007), 1579–1588.

[Philips Adewuyi et al. 2009] A. Philips Adewuyi, Z. Wu, and N. H. M. Kammrujaman Serker, "Assessment of vibration-based damage identification methods using displacement and distributed strain measurements", *Struct. Health Monit.* **8**:6 (2009), 443–461.

[Sadílek and Zemčík 2010] P. Sadílek and R. Zemčík, "Frequency response analysis of hybrid piezoelectric cantilever beam", *Eng. Mech.* **17**:2 (2010), 73–82.

[Sekhar 2008] A. S. Sekhar, "Multiple cracks effects and identification", *Mech. Syst. Signal Process.* **22**:4 (2008), 845–878.

[Sinha et al. 2002] J. K. Sinha, M. I. Friswell, and S. Edwards, "Simplified models for the location of cracks in beam structures using measured vibration data", *J. Sound Vib.* **251**:1 (2002), 13–38.

[Sulbhewar and Raveendranath 2015] L. N. Sulbhewar and P. Raveendranath, "A numerically accurate and efficient coupled polynomial field interpolation for Euler–Bernoulli piezoelectric beam finite element with induced potential effect", *J. Intell. Mater. Syst. Struct.* **26**:12 (2015), 1539–1550.

[Verhese and Shankar 2014] C. K. Verhese and K. K. Shankar, "Damage identification using combined transient power flow balance and acceleration matching technique", *Struct. Control Health Monit.* **21**:2 (2014), 135–155.

[Viola et al. 2001] E. Viola, L. Federici, and L. Nobile, "Detection of crack location using cracked beam element method for structural analysis", *Theor. Appl. Fract. Mech.* **36**:1 (2001), 23–35.

[Viola et al. 2002] E. Viola, L. Nobile, and L. Federici, "Formulation of cracked beam element for structural analysis", *J. Eng. Mech. (ASCE)* **128**:2 (2002), 220–230.

[Wang et al. 2001] X. Wang, N. Hu, H. Fukunaga, and Z. H. Yao, "Structural damage identification using static test data and changes in frequencies", *Eng. Struct.* **23**:6 (2001), 610–621.

[Xu and ShengPeng 2013] L. Xu and S. ShengPeng, "Dynamic analysis of Bernoulli–Euler piezoelectric nanobeam with electrostatic force", *Sci. China G Phys. Mech. Astronom.* **56**:10 (2013), 1930–1937.

[Yang and Wang 2010] Z. Yang and L. Wang, "Structural damage detection by changes in natural frequencies", *J. Intell. Mater. Syst. Struct.* **21**:3 (2010), 309–319.

[Zemčík and Sadílek 2007] R. Zemčík and P. Sadílek, "Modal analysis of beam with piezoelectric sensors a actuators", *Appl. Comput. Math.* **1** (2007), 381–386.

NARAYANAN JINESH: jineshkarthi@gmail.com
Department of Mechanical Engineering, Indian Institute of Technology, Chennai, India

KRISHNAPILLAI SHANKAR: skris@iitm.ac.in
Department of Mechanical Engineering, Indian Institute of Technology, Chennai, India

JOURNAL OF MECHANICS OF MATERIALS AND STRUCTURES

msp.org/jomms

Founded by Charles R. Steele and Marie-Louise Steele

Cover photo: Mando Gomez, www.mandolux.com

Journal of Mechanics of Materials and Structures

Volume 13, No. 2   March 2018